Journal of Molecular Catalysis A: Chemical 332 (2010) 32–44

Contents lists available at ScienceDirect

Journal of Molecular Catalysis A: Chemical

journal homepage: www.elsevier.com/locate/molcata

# Catalytic behaviors of CuO supported on $Mn_2O_3$ modified γ-$Al_2O_3$ for NO reduction by CO

Haiqin Wan[a], Dan Li[b], Yue Dai[b], Yuhai Hu[b], Bin Liu[b], Lin Dong[b,*]

[a] State Key Laboratory of Pollution Control and Resource Reuse, School of Environment, Nanjing University, Nanjing 210093, China
[b] Key Laboratory of Mesoscopic Chemistry of MOE, School of Chemistry and Chemical Engineering, Nanjing University, Nanjing 210093, China

ARTICLE INFO

*Article history:*
Received 10 February 2010
Received in revised form 26 July 2010
Accepted 12 August 2010
Available online 20 August 2010

*Keywords:*
CuO/γ-$Al_2O_3$
Manganese oxide
Modification
Dispersion capacity
Epitaxial growth
In situ IR
NO
CO

ABSTRACT

CuO supported on γ-$Al_2O_3$ and $Mn_2O_3$ modified γ-$Al_2O_3$ was prepared and characterized by XRD, UV–vis, XPS, TPR and in situ adsorption IR. NO reduction by CO over these catalysts was also investigated. For the modification of γ-$Al_2O_3$ by $Mn_2O_3$, manganese oxide was highly dispersed on γ-$Al_2O_3$ surface to form a monolayer with a dispersion capacity of about 1.0 mmol $Mn^{3+}$/100 $m^2$ γ-$Al_2O_3$ corresponding to 8.1 wt.% of Mn. For supported copper oxide, CuO dispersion capacity was 0.75 mmol $Cu^{2+}$/100 $m^2$ γ-$Al_2O_3$ on γ-$Al_2O_3$, and increased to 1.1 mmol $Cu^{2+}$/100 $m^2$ γ-$Al_2O_3$ on 1.0 $MnO_x$–γ-$Al_2O_3$, indicative of an elevated CuO dispersion capacity upon $Mn_2O_3$ modification. For NO reduction by CO, the addition of manganese oxide generally enhanced NO conversion and $N_2$ selectivity. Furthermore, the catalyst with the loading amounts of Cu and Mn of 0.6 mmol and 0.3/100 $m^2$ γ-$Al_2O_3$ respectively exhibited the most prominent catalytic efficiency among the tested catalysts in terms of NO conversion and $N_2$ selectivity. Additionally, these catalysts showed stable NO conversion and $N_2$ selectivity.



## 1. Introduction

The emission of $NO_x$ from both mobile and stationary sources is a serious environmental problem because nitrogen oxides bring about acid rain, photochemical smog, ozone destruction and green house effects. Several methods have been developed for $NO_x$ removal to meet the increasingly stringent regulations on nitrogen oxide emissions. Selective catalytic reduction (SCR) of $NO_x$ has been considered to be the most popular technique among $NO_x$ abatement technologies like storage and thermal decomposition. The most common reductants for SCR are ammonia, urea, $H_2$, CO and hydrocarbons like methane, ethane and propylene. Carbon monoxide as a reductant offers some distinct advantages since it can be produced onsite for the cases of coal or natural gas utilization (stationary sources), or it is part of the exhaust stream due to incomplete combustion of the liquid fuel (mobile sources). The catalytic reduction of NO by CO has been studied extensively and the supported noble metal (Pt, Pd, Rh, Ir or Au) catalysts exhibit high catalytic activity [1–6], but the cost of the noble metal is rather expensive. Therefore, supported transition metal oxides provide an alternative catalyst for the reduction of NO by CO, and among which manganese-based catalysts and copper-based catalysts have received increasing attention [7–10].

In recent years, $MnO_x$-based catalysts attracted much attention due to high activity for catalytic removal of NO. The reactions including the reduction of NO by $NH_3$ over $Mn_3O_4$ and $Mn_2O_3$ [11], and that by CO, $H_2$, and $NH_3$ over MnO [12] and $MnO_2$ [13], the decomposition of NO and $N_2O$ over MnO, $MnO_2$, $Mn_3O_4$ and $Mn_2O_3$ [14,15] were widely investigated. Even though these oxides indicate different activities and have various types of labile oxygen that are necessary to complete a catalytic cycle, the reactions were generally operated at higher temperature to enable the reduction of manganese oxide to take place.

Copper oxide based catalysts are generally considered to be highly active for NO reduction by CO. Copper oxide has been supported on different supports, such as $CeO_2$, $ZrO_2$, $TiO_2$, γ-$Al_2O_3$, and zeolite or prepared to spinel oxide, i.e., $CuCoO_x$ and $CuMnO_x$. Among these catalysts, CuO/γ-$Al_2O_3$ indicates potential application in practical reaction in terms of NO conversion. The catalytic behaviors of CuO are strongly dependent on support properties. For example, Nickolov et al. [16] have modified γ-$Al_2O_3$ support by carbon in the CuO/γ-$Al_2O_3$ catalyst, and they found that carbon can prevent the aggregation of copper oxide and improve the catalytic activity. Pineda et al. [17] have prepared $Al_2O_3$–$TiO_2$ mixed

* Corresponding author at: College of Chemistry and Chemical Engineering, Department of Chemistry, Hankou Road 22#, Nanjing, Jiangsu 210093, China. Tel.: +86 25 83594945; fax: +86 25 83317761.
*E-mail address:* donglin@nju.edu.cn (L. Dong).

1381-1169/$ – see front matter © 2010 Elsevier B.V. All rights reserved.
doi:10.1016/j.molcata.2010.08.016

oxide as support considering the reducibility of $TiO_2$, and they concluded that there is a reducing cycle $Ti^{4+}$ to $Ti^{3+}$ and $Cu^{+}$ to $Cu^{2+}$ which is beneficial for the NO reduction by CO. Jiang et al. [18] and Khristova et al. [19] have modified γ-$Al_2O_3$ with $CeO_2$ individually, found that $CeO_2$ can promote the activity of the catalysts due to the redoxy cycle between $CeO_2$ and CuO, i.e., $Ce^{4+}$ to $Ce^{3+}$ and $Cu^{+}$ to $Cu^{2+}$. Moreover, cobalt oxide or manganese oxide has been introduced into this catalyst to improve the catalytic activity [20–22]. It should be noted that the oxidation state of Mn in manganese oxide is labile, and there will be a redoxy cycle between $MnO_x$ and CuO as manganese oxide was introduced into CuO/γ-$Al_2O_3$ catalysts. However, copper oxide supported on manganese oxide modified γ-$Al_2O_3$ has been seldom addressed.

Mixed copper–manganese oxide has been proved to indicate high activity toward the oxidation of carbon monoxide [23,24] and NO reduction by CO [25] at ambient temperature. Spassova et al. [25] attributed the high activity for the NO–CO reaction to the formation of a disordered mixed oxide with a spinel-like structure. Nonetheless, the copper–manganese mixed oxide loses activity for CO oxidation at around 500 °C. This was assumed to be a result of crystallization of $CuMn_2O_4$ from the more active amorphous state [26–28]. Mixed copper–manganese oxide has been studied extensively in the past decades [24,25,27,29,30], catalysts with mixed copper–manganese oxides supported on the γ-$Al_2O_3$ remain little studied [31]. In this paper, influence of manganese oxide on the activities of CuO/γ-$Al_2O_3$ catalysts in NO reduction by CO was studied. CuO/$MnO_x$–γ-$Al_2O_3$ samples were prepared by stepwise impregnation method and the reaction NO reduction by CO over these catalysts was investigated to evaluate the influence of $MnO_x$ as a modifier on the catalytic behavior of CuO/γ-$Al_2O_3$ catalyst.

## 2. Experimental

### 2.1. Catalyst preparation

γ-$Al_2O_3$ support, obtained from Fushun Petrochemical Institute of China, was calcined in flowing air at 700 °C for 7 h and the BET surface area was determined to be 160.8 $m^2\,g^{-1}$. $MnO_x$–γ-$Al_2O_3$ samples were prepared by wet impregnating γ-$Al_2O_3$ with aqueous $Mn(CH_3COO)_2$ solution containing required $MnO_x$ contents. The samples were dried at 110 °C overnight, and then calcined at 500 °C for 5 h in air [32,33]. The resultant samples are denoted as *y*Mn–Al, e.g., 0.3Mn–Al corresponds to a $MnO_x$–γ-$Al_2O_3$ sample with a manganese oxide loading amount of 0.3 mmol $Mn^{3+}$/100 $m^2$ γ-$Al_2O_3$.

CuO/$MnO_x$–γ-$Al_2O_3$ catalysts were prepared by impregnating Mn–Al sample with aqueous $Cu(NO_3)_2$ solution containing requisite amount of CuO. The samples were dried at 110 °C overnight, and then calcined at 500 °C for 5 h in air. The obtained catalysts are referred to as *x*Cu/*y*Mn–Al, e.g., 0.6Cu/0.3Mn–Al corresponds to the CuO/$MnO_x$–γ-$Al_2O_3$ catalyst with $Cu^{2+}$ and $Mn^{3+}$ loading amounts of 0.6 and 0.3 mmol/100 $m^2$ γ-$Al_2O_3$, respectively.

### 2.2. Catalyst characterization

X-ray diffraction (XRD) patterns of the catalysts were recorded on a Philips X'pert Pro diffractometer using Ni-filtered Cu Kα radiation (λ = 0.15418 nm). The X-ray tube was operated at 40 kV and 40 mA. The UV–vis spectra of the samples were recorded on a SHIMAD UV-2401PC UV–vis spectrometer in diffuse reflectance mode in the range of 200–800 nm, at room temperature, using $BaSO_4$ as a reference. X-ray photoelectron spectra (XPS) measurements were performed on a Thermo ESCALAB 250 high performance electron spectrometer using monochromatized Al Kα ($h\nu$ = 1486.6 eV) as the excitation source. The binding energy (BE) of C 1s level (284.6 eV) was used as the internal reference.

Temperature programmed reduction (TPR) was carried out on a homemade apparatus consisting of a gas chromatograph with a thermal conduction detector (TCD). Typically, 100 mg of the sample was pressed into wafers, broken into small platelets (20–40 mesh), and charged into a quartz reaction tube. The sample was pretreated at 100 °C in a $N_2$ flow for 1 h. After cooled to room temperature, the sample was heated from room temperature to 500 °C under a flow gas consisting of 7% $H_2$ in Ar (30 mL/min) at a ramping rate of 10 °C/min.

In situ infrared spectra (IR) of CO adsorption on the catalysts were recorded on a Nicolet 5700 FT-IR spectrometer at a spectral resolution of 4 $cm^{-1}$. The sample was pressed into a self-supporting wafer (about 10 mg), and mounted in a commercial controlled environment chamber (HTC-3). The wafer was pretreated at 100 °C in a high pure $N_2$ flow for 1 h. After cooled to room temperature, the catalyst was subjected to adsorption under a flow gas consisting of 10% CO in $N_2$ (5 mL/min) for 30 min. IR spectra were recorded at various target temperatures and the difference spectra were obtained by subtracting the IR spectra of CO background gas recorded at corresponding temperatures. IR spectra of NO and NO–CO co-adsorption on the catalysts were obtained by a similar way as that of CO adsorption with exception that a stream of CO–NO mixture (2:1 by volume) was used with the background of CO–NO mixture (without catalysts) at the corresponding temperatures subtracted.

### 2.3. Catalytic tests

NO reduction by CO was carried out at atmospheric pressure in a fixed bed quartz micro-reactor (i.d. 6 mm). Typically, 25 mg (20–40 mesh) of the catalyst was placed in the reactor. The feed gas consisted of 5% NO, 10% CO and 85% He by volume at a space velocity of 24,000 mL $g^{-1}$ $h^{-1}$. Prior to the catalytic tests, the catalysts were activated in a $N_2$ stream at 100 °C for 1 h. The reactants and products were analyzed using an on-line gas chromatograph equipped with a TCD detector, and Porapak Q column for the separation of $N_2O$ and $CO_2$ and 5A molecular sieve (30–60 mesh) for the separation of $N_2$, NO and CO.

## 3. Results and discussion

### 3.1. X-ray diffraction

Fig. 1(A) shows XRD patterns of γ-$Al_2O_3$ and *y*Mn–Al samples with varied manganese oxide loading amounts. At the manganese oxide loading amounts lower than 1.2 mmol $Mn^{3+}$/100 $m^2$ γ-$Al_2O_3$, only XRD diffraction peaks with 2$\theta$ at 32.6°, 37.0°, 45.7°, 67.0° were observed, attributed to γ-$Al_2O_3$ support. As the manganese oxide loading amounts increased from 1.2 to 2.4 mmol $Mn^{3+}$/100 $m^2$ γ-$Al_2O_3$, additional XRD diffraction peaks with 2$\theta$ at 32.4° and 36.2° were clearly visible, characteristic of crystalline $Mn_2O_3$ [PDF-ICDD] (card no. 06-0540). In addition, the intensities of the diffraction peaks increased with the manganese oxide loadings. To clarify the dispersion behavior of $Mn_2O_3$ over γ-$Al_2O_3$, quantitative XRD analysis was conducted by measuring the ratio of the peak area of crystalline $Mn_2O_3$ at 36.2° to that of γ-$Al_2O_3$ support at 45.7° as a function of $Mn_2O_3$ loading [34,35] and the result is shown in Fig. 1(B). The dispersion capacity is equal to the intercept of linear extrapolation to manganese oxide loading axis and the resultant dispersion capacity of manganese oxide on γ-$Al_2O_3$ is 1.0 mmol $Mn^{3+}$/100 $m^2$ γ-$Al_2O_3$, which is in good agreement with the predicted value (1.0 mmol $Mn^{3+}$/100 $m^2$ γ-$Al_2O_3$) using the incorporation model proposed by Chen and Zhang [36]. Similar monolayer dispersion amount was also reported by Zhu et al. [37] (1.1 mmol $Mn^{3+}$/100 $m^2$ γ-$Al_2O_3$).

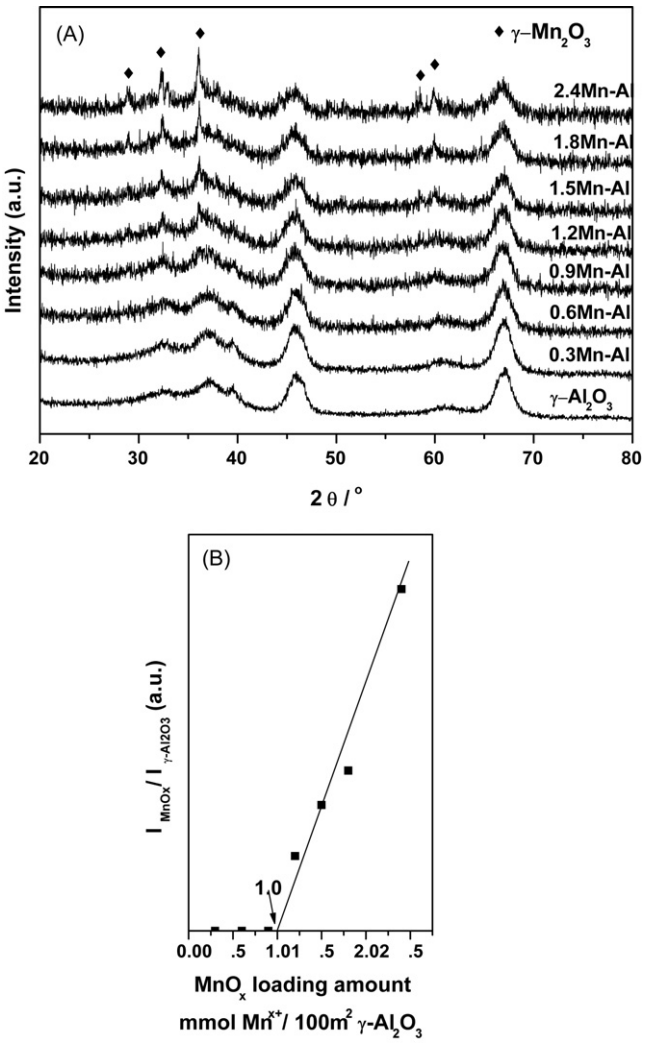


**Fig. 1.** XRD patterns of various Mn–Al samples (A) and the quantitative XRD results of Mn–Al samples (B).

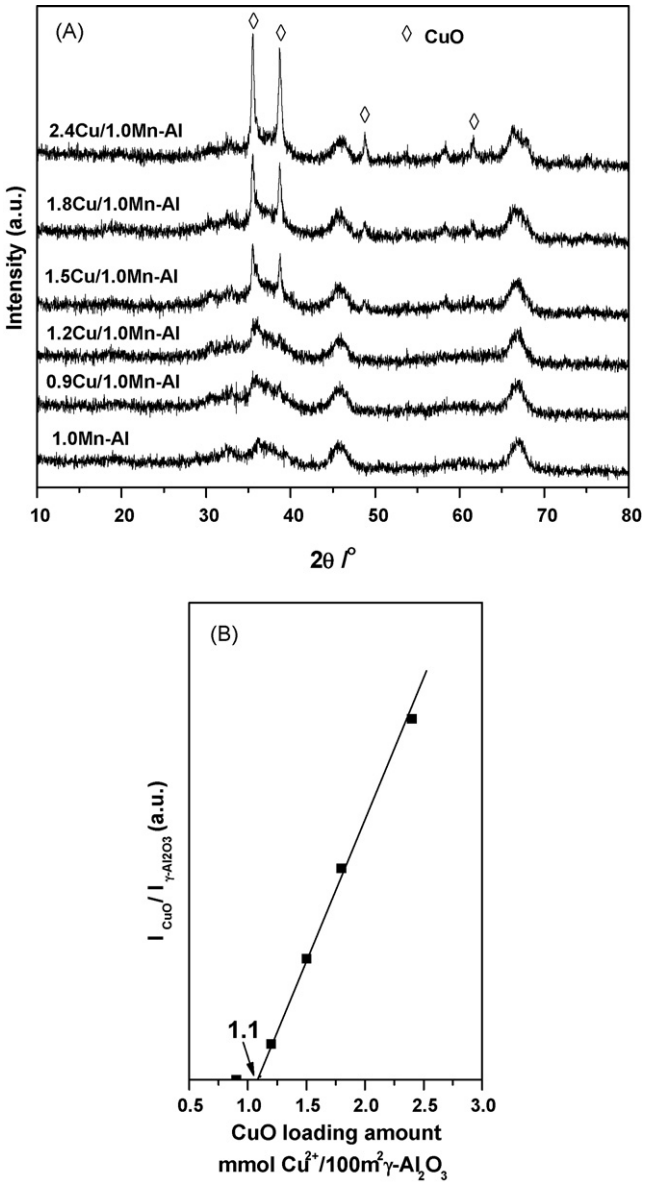


**Fig. 2.** XRD patterns of various Cu/1.0Mn–Al samples (A) and the quantitative XRD results of Cu/1.0Mn–Al samples (B).

After the modification of $\gamma$-$Al_2O_3$ by $MnO_x$, copper oxide dispersion behavior on Mn–Al may differ on $\gamma$-$Al_2O_3$. Therefore, the dispersion capacity of copper oxide on the 1.0Mn–Al sample was also measured by XRD, and the results are shown in Fig. 2. Panel (A) shows XRD patterns of *x*Cu/1.0Mn–Al samples. No characteristic peaks in association with crystalline copper oxide were observed at the loading amounts of copper oxide below 1.2 mmol $Cu^{2+}$/100 $m^2$ $\gamma$-$Al_2O_3$. As the loading amounts of copper oxide increased to 1.2 mmol $Cu^{2+}$/100 $m^2$ $\gamma$-$Al_2O_3$, XRD diffraction peaks characteristic of crystalline CuO ($2\theta$ = 35.5°, 38.7°) [PDF-ICDD] (card no. 41-0254) were observed. Similarly, the CuO dispersion capacity was calculated by quantitative XRD analysis by determining the ratio of the peak area of crystalline CuO at 38.7° to that of $\gamma$-$Al_2O_3$ support at 45.7° as a function of CuO loading, and as shown in Fig. 2(B) the dispersion capacity of CuO on the 1.0Mn–Al is found to be about 1.1 mmol $Cu^{2+}$/100 $m^2$ $\gamma$-$Al_2O_3$. It is noteworthy that the dispersion capacity of copper oxide on $\gamma$-$Al_2O_3$ was 0.75 mmol $Cu^{2+}$/100 $m^2$ $\gamma$-$Al_2O_3$ [38], indicative of a substantially increased dispersion capacity of copper oxide on manganese oxide modified $\gamma$-$Al_2O_3$ in comparison with that on $\gamma$-$Al_2O_3$.

In general, for the supported metal oxide catalysts, the catalytic properties of metal oxide and the interaction between metal oxide and support are associated with metal oxide loading amount. Moreover, the catalytic properties of the supported metal oxide can be tuned by modifying the support [39]. To investigate the influence of manganese oxide loading on the catalytic properties of Cu/Al catalysts, a low loading (0.3 mmol) and a near half monolayer loading (0.6 mmol) of manganese oxide were used to modify the $\gamma$-$Al_2O_3$ support. A low loading (0.3 mmol), near dispersion capacity loading (0.6 mmol) and a high loading (1.2 mmol) of copper oxide with Mn–Al samples as the supports were selected to assess the catalytic behaviors of Cu/Mn–Al catalysts for NO reduction by CO. Fig. 3 shows XRD patterns of the Cu/Mn–Al catalysts. For all of the catalysts, no XRD characteristic peaks in association with crystalline manganese oxide at the manganese oxide loading amounts were detectable in this study ($\leq$0.6 mmol $Mn^{3+}$/100 $m^2$ $\gamma$-$Al_2O_3$) while the characteristic peaks of crystalline CuO were observed with $2\theta$ at 35.5° and 38.7° [PDF-ICDD] (card no. 41-0254) were observed only with the copper oxide loading at 1.2 mmol, and the intensities of these peaks diminished substantially with increasing the loading amount of manganese oxide. It indicates that the presence of preloaded manganese oxide, irrespective of the loading of manganese oxide, promotes the dispersion of copper oxide.

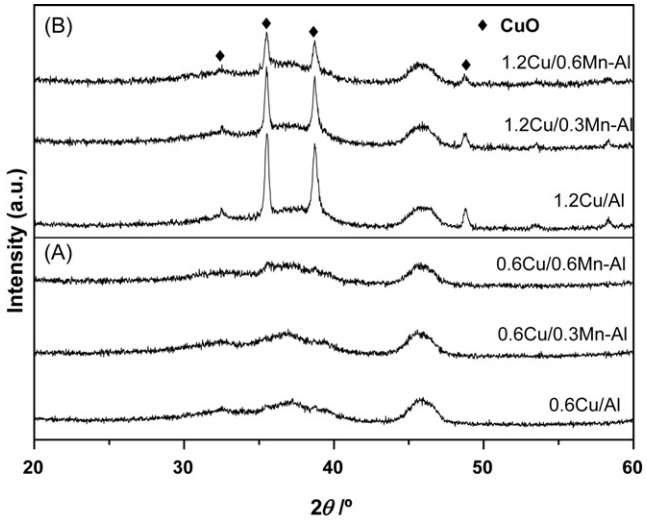


**Fig. 3.** XRD patterns of various Cu/Mn–Al catalysts.

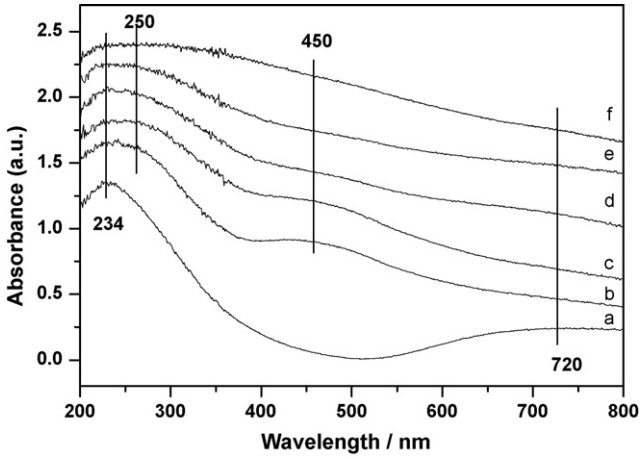


**Fig. 4.** UV–vis spectra of the catalysts: (a) 0.6Cu/Al, (b) 0.3Mn–Al, (c) 0.6Mn–Al, (d) 0.6Cu/0.3Mn–Al, (e) 0.6Cu/0.6Mn–Al, and (f) 0.6Cu/1.0Mn–Al.

As previously reported, the dispersion capacity of copper oxide on the modified γ-$Al_2O_3$ is suppressed at the loading of modifier lower than its dispersion capacity. For example, the dispersion capacities of copper oxide on 0.6Mg/Al and 0.13Ti/Al are 0.15 and 0.58 mmol $Cu^{2+}$/100 $m^2$ γ-$Al_2O_3$, respectively [40,41]. However, the dispersion capacity of copper oxide on the $Mn_2O_3$ modified γ-$Al_2O_3$ is enhanced. The reason for the change in the dispersion capacity of CuO may be that an epitaxial layer of $Mn_2O_3$ was formed on the surface of γ-$Al_2O_3$ and the tetrahedral vacancy sites of $Mn_2O_3$ epitaxial layer were occupied by the $Cu^{2+}$ ions. Because $Mn_2O_3$ has several lattice structures, among which, γ-$Mn_2O_3$ has the same structure with γ-$Al_2O_3$, thus, it is easier for $Mn_2O_3$ to grow as an epitaxil layer on the surface of γ-$Al_2O_3$ under the inducement of the support surface. This opinion is also supported by Kapteijn et al. [33]. Another factor which should be taken into consideration is that strong interaction exists between copper oxide and manganese oxide. This interaction leads to the formation of Cu–Mn spinel [25,27]. Additionally, Faungnawakij et al. [42] pointed out that $Cu^{2+}$ occupied the tetrahedral vacant sites of the $Mn_2O_3$.

### 3.2. UV–vis spectra

To gain further information on the state of Cu and Mn species in these catalysts, the UV–vis spectroscopic studies were carried out and the spectra are shown in Fig. 4. For 0.6Cu/Al, two strong absorption bands centered at about 234 and 720 nm were observed, as shown in Fig. 4 curve a, which can be assigned to the charge-transfer from $O^{2-} \rightarrow Cu^{2+}$ and d–d transitions of $Cu^{2+}$ situated in the octahedral environment, respectively [40,43,44]. It suggests that $Cu^{2+}$ ions occupied the octahedral vacancy sites of γ-$Al_2O_3$ in Cu/Al samples which is consistent with the previous result [36]. For 0.3Mn–Al and 0.6Mn–Al (curves b and c), a main absorption band centered at about 250 nm and a wide band of lower intensity centered at about 450 nm. Parida et al. [45] observed a similar band at 270 nm in Mn-MCM-41. They attributed the band at about 270 nm to the charge-transfer transition of $O^{2-} \rightarrow Mn^{3+}$ in octahedral coordination. Kijlstra et al. [46] observed the band at about 445 nm in Mn–γ-$Al_2O_3$ sample, and assigned it to the $^5T_{2g} \rightarrow {}^5E_g$ of $Mn^{3+}$. Combining the XRD and UV–vis results, it is reasonable to conclude the oxidation state of manganese is main $Mn^{3+}$ in this system. This is consistent with the result reported by Kapteijn et al. [33]. For the 0.6Cu/*y*Mn–Al, as the value of *y* at 0.3 and 0.6 (curves d and e), four absorption bands centered at about 234, 250, 450 and 720 nm were detected, indicating that the states of Cu and Mn species in the two component catalysts are basically consistent with those in their single component catalysts. However, the intensity of the bands at about 720 nm was decreased obviously as compared to that of the 0.6Cu/Al sample which means that the amount of the $Cu^{2+}$ ions decreased in the octahedral environment. It should be noted that, as the value of *y* was at 1.0 (curve f), the absorption band centered at about 720 nm disappeared, indicating that no octahedral environment Cu species were observed. This result suggests that $Cu^{2+}$ ions preferentially occupied the octahedral vacancy sites of γ-$Al_2O_3$ while preferentially occupied the tetrahedral vacancy of the $Mn_2O_3$ epitaxial layer.

According to the incorporation model a schematically graph was proposed to describe the change of the dispersion capacity and the states of copper oxide on the $Mn_2O_3$ modified γ-$Al_2O_3$. Since the preferentially exposed plane of γ-$Al_2O_3$ is (1 1 0), two kinds of stacking patterns named C- and D-layer and the exposing possibilities of these two layers are equal [47]. According to the lattice structure of γ-$Al_2O_3$, Schuit et al. have simplified the (1 1 0) plane by assuming to consist of particles formed by one-dimensional stacking of C- and D-layer [47]. The epitaxil growth means that a new $Mn_2O_3$ layer forms on the surface of γ-$Al_2O_3$ when manganese oxide is pre-dispersed on it. The characteristic of the (1 1 0) plane of γ-$Al_2O_3$ is stacked as CDCDCD……, so, as $M_2O_3$ dispersed on C-layer of γ-$Al_2O_3$, a D-layer of $Mn_2O_3$ forms. In contrast, as $Mn_2O_3$ dispersed on D-layer of γ-$Al_2O_3$, a new C-layer $Mn_2O_3$ forms. There are two kinds of vacant sites on the preferentially exposed (1 1 0) plane of γ-$Al_2O_3$, i.e., octahedral and tetrahedral sites [48,49]. When calcination temperature is below 750 °C, the dispersion capacity of copper oxide on γ-$Al_2O_3$ is 0.75 mmol $Cu^{2+}$/100 $m^2$ γ-$Al_2O_3$ due to the fact that $Cu^{2+}$ only occupies octahedral sites [38,48]. As manganese oxide is pre-dispersed, an epitaxil layer is formed and $Cu^{2+}$ ions occupy the tetrahedral vacancy sites of the $Mn_2O_3$ surface. For the C-layer of γ-$Al_2O_3$, CuO and $Mn_2O_3$ dispersed as shown in Fig. 5 (A)–(D). For the D-layer of γ-$Al_2O_3$, see Fig. 5(E)–(H) for dispersion. It should be illustrated that only part of tetrahedral vacancy sites were occupied by considering the shielding effect of the capping oxygen [36,48]. From Fig. 5(C) and (G), it can be found that 4 and 2 tetrahedral vacancy sites were occupied by $Cu^{2+}$ in a unit mesh (the region in the rectangle), respectively. According to the incorporation mode, the dispersion capacity of CuO on 1.0Mn–Al is calculated as follows: generally, the lattice structure of γ-$Al_2O_3$ is cubic system. Setting the rectangle marked as *MNOP* (shown as Fig. 5(A)) stands for the unit mesh. Setting the length of the cube side as *a*, the radius of the $O^{2-}$ as *r* and the distance between two neighbor $O^{2-}$ ions in *MP* side as *x*, that

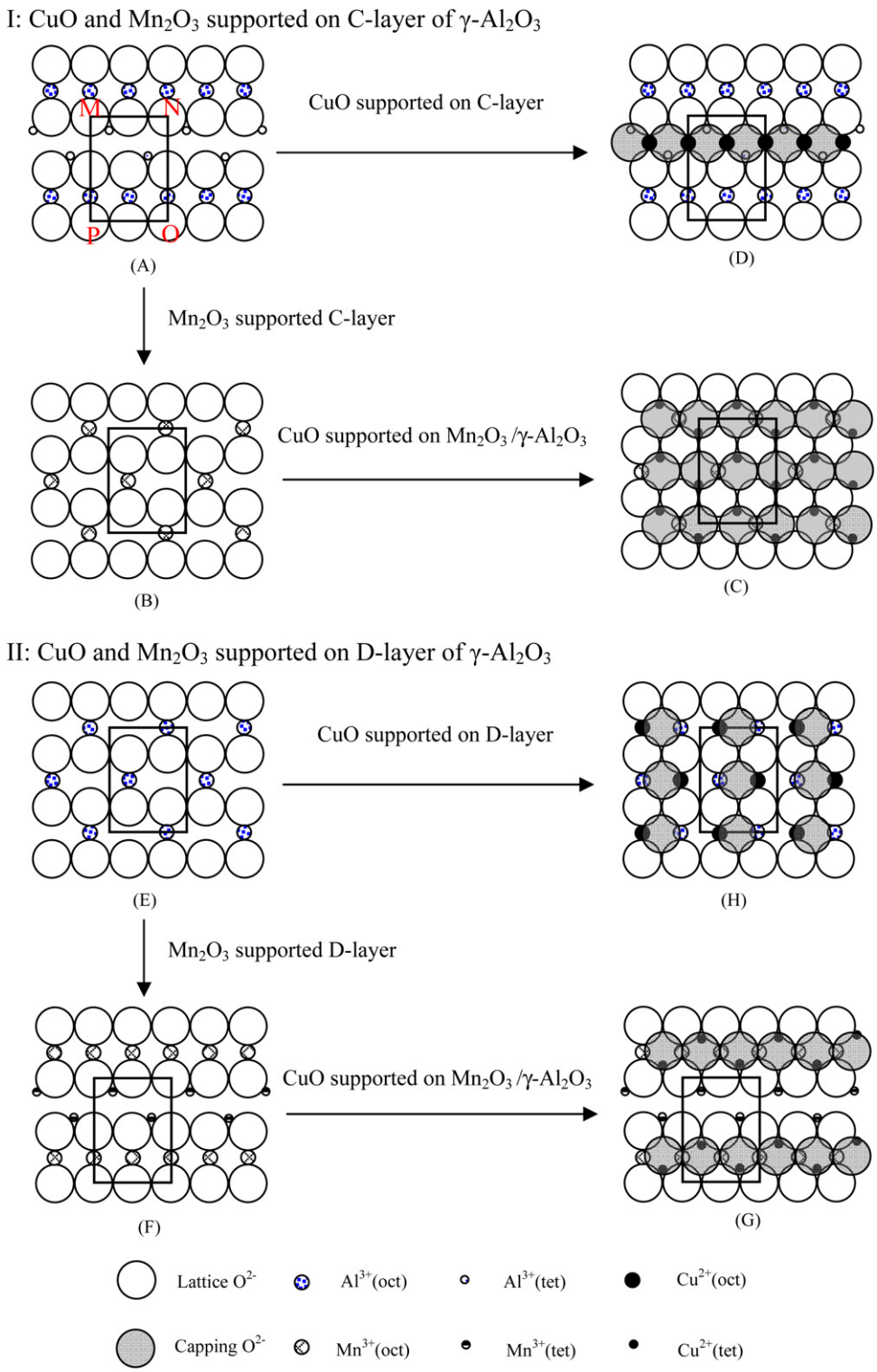


**Fig. 5.** The schematic mode for the dispersion of copper oxide on the surface of γ-$Al_2O_3$ and manganese oxide modified γ-$Al_2O_3$.

the length of the unit mesh

$$MN = 4r = \sqrt{2}a \quad (1)$$

$$MP = 4r + 2x = 2a \quad (2)$$

Solve Eqs. (1) and (2), $x = 0.838r$. Setting the radius of $O^{2-}$ as 0.14 nm, the unit mesh area is about 0.443 $nm^2$. Then the amount of the occupied tetrahedral vacancy sites per 100 $m^2$ support is:

$$n = \frac{100\ m^2}{0.443\ nm^2} \times \frac{1}{2}(4+2) \times \frac{1}{Na} \quad (3)$$

Here, 4 and 2 stand for the number of the occupied tetrahedral vacancy sites in the unit mesh of D-layer and C-layer of $Mn_2O_3$ respectively. The average is adopted because the exposed possibility of C-layer and D-layer is equal. *Na* stands for the Avogadro's constant ($6.02 \times 10^{23}\ mol^{-1}$). It can be calculated that the amount of

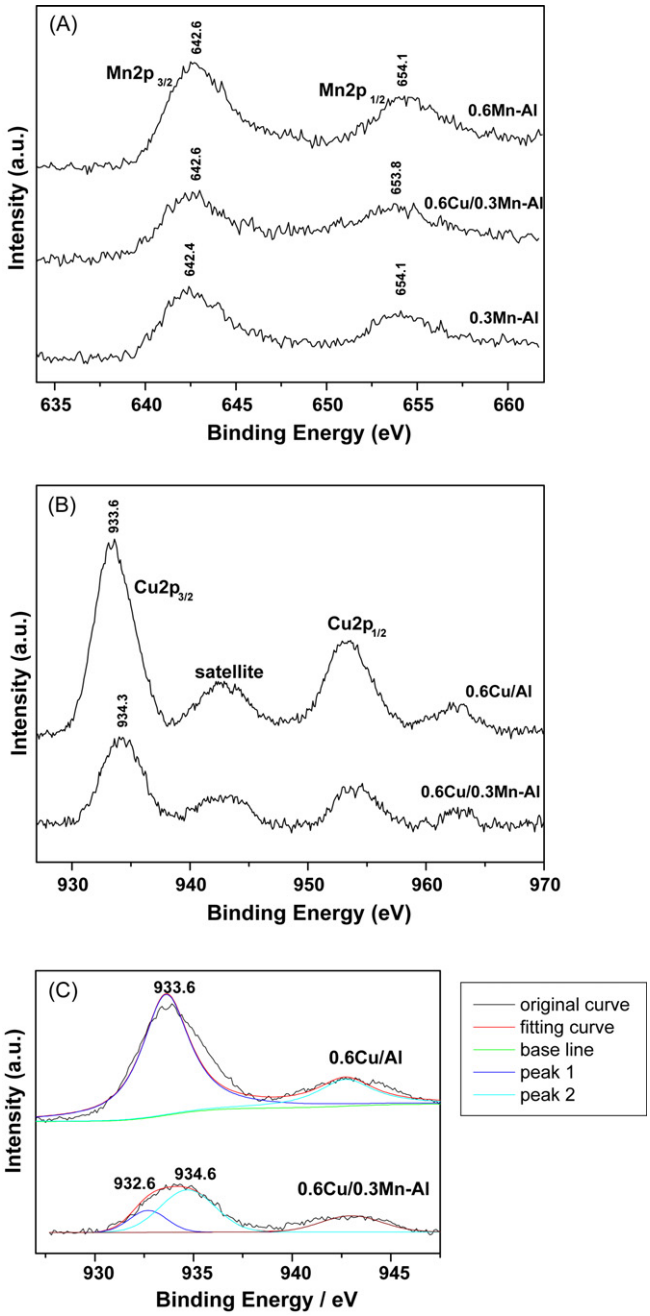


**Fig. 6.** XP-spectra of selected Cu/Mn–Al catalysts (A) Mn2p results of 0.3Mn–Al, 0.6Mn–Al and 0.6Cu/0.3Mn–Al; (B) Cu2p results of 0.6Cu/Al and 0.6Cu/0.3Mn–Al; (C) Peak fitting results of 0.6Cu/Al and 0.6Cu/0.3Mn–Al.

occupied tetrahedral vacancy sites is 1.12 mmol/100 $m^2$ 1.0Mn–Al. The calculating result is in good agreement with the experiment result as shown in Fig. 2(B). Therefore, the fact that pre-dispersed manganese oxide promotes the dispersion capacity of CuO on the $\gamma$-$Al_2O_3$ surface is explained by the epitaxial layer of $Mn_2O_3$.

### 3.3. X-ray photoelectron spectra

Fig. 6 shows the XPS spectra of the Cu/Mn–Al catalysts. The concentrations of surface atoms were also calculated and the results are listed in Table 1. As shown in Fig. 6(A), the binding energies of Mn $2p_{3/2}$ and Mn $2p_{1/2}$ in the presence and absence of CuO were found to be around 642.6 and 654.1 eV respectively, suggesting a minor change in chemical valence of $MnO_x$ upon CuO loading. Previous studies indicated that the binding energies of Mn $2p_{3/2}$ in crystalline $MnO_2$, $Mn_2O_3$, $Mn_3O_4$, MnO and $MnAl_2O_4$ are 641.1–642.4, 641.2–641.9, 641.3–641.4, 640.6–641.7, and 641.6 eV, respectively [50–53]. However, Kapteijn et al. [33] reported that the binding energy of Mn $2p_{3/2}$ in $MnO_x/\gamma$-$Al_2O_3$ sample (4.5 wt.% of Mn) prepared using acetate as the precursor was about 1.0–1.5 eV higher than the crystalline manganese oxide, giving rise to a binding energy of around 642.4 eV. They concluded that $Mn_2O_3$ was the predominant species in $MnO_x/\gamma$-$Al_2O_3$ sample, and the slightly higher binding energy mainly resulted from the high dispersion of manganese oxide on $\gamma$-$Al_2O_3$ surface. In the tested Mn–Al and Cu/Mn–Al samples, therefore, manganese oxide mainly exists as highly dispersed $Mn_2O_3$ as indicated by XRD characterization. The conclusion is also supported by XPS analysis of the surface concentration of Mn atoms in the samples. As shown in Table 1, increasing the loading amount of manganese oxide from 0.3 to 0.6 mmol $Mn^{3+}$/100 $m^2$ $\gamma$-$Al_2O_3$ led to the increase of the concentration of Mn atoms from 1.69% to 3.15%. The surface Mn concentrations detected by XPS are proportional to Mn loading, suggesting an almost identical $Mn_2O_3$ dispersion.

**Table 1**
Surface atom percent of Cu/Mn–Al catalysts from XPS results.

| Samples | $Al^{3+}$ (at.) | $Mn^{3+}$ (at.) | $Cu^{2+}$ (at.) | $O_2$ (at.) |
|---|---|---|---|---|
| 0.3Mn–Al | 24.73% | 1.69% | | 73.58% |
| 0.6Cu/0.3Mn–Al | 21.18% | 2.15% | 3.07% | 73.6% |
| 0.6Mn–Al | 22.14% | 3.15% | | 74.35% |
| 0.6Cu/Al | 29.47% | | 3.7% | 66.83% |

XPS analysis of surface CuO was also conducted and the results are presented in Fig. 6(B). In contrast to $Mn_2O_3$, the binding energies of Cu $2p_{3/2}$ in 0.6Cu/Al and 0.6Cu/0.3Mn–Al were found to be 933.6 and 934.3 eV, indicating a substantially increased binding energy of CuO upon $Mn_2O_3$ modification. For CuO/$\gamma$-$Al_2O_3$, the binding energy at 933.6 eV is associated with the location of typical $Cu^{2+}$ [54,55]. Severino et al. [56] studied the nature of the copper species present on the surface of $CuAl_2O_4$ catalyst, and concluded that the binding energy of $Cu^{2+}$ incorporated into tetrahedral coordinated sites (A-type sites of the $CuAl_2O_4$ spinel structure) was 935.3 eV, substantially larger as compared to that incorporated into octahedral coordinated sites. It is noteworthy that no new crystalline phases were observed in the Cu/Mn–Al catalysts as indicated by XRD analysis. Therefore, the increased binding energy of Cu resulting from $Mn_2O_3$ modification could be attributed to the occupation of $Cu^{2+}$ in the tetrahedral vacancy sites in Cu/Mn–Al catalysts. This result is consistent the UV–vis result and confirms the description of Fig. 5(C) and (G). It should be noted that the peak of Cu $2p_{3/2}$ is broadened with the $Mn_2O_3$ modification. Therefore, the peak fittings of Cu $2p_{3/2}$ of 0.6Cu/Al and 0.6Cu/0.3Mn–Al were carried out and the results are shown in Fig. 6(C). Only one peak at 933.6 eV resulted from the Cu $2p_{3/2}$ of 0.6Cu/Al but two peaks at 932.6 and 934.6 eV from that of 0.6Cu/0.3Mn–Al. The lower binding energy (932.2–933.1 eV) and the absence of shake-up peaks is characteristic for $Cu^+$ [56–58]. This indicates that some $Cu^+$ species are formed in the Cu/Mn–Al catalysts. This can be assigned to the radiation of X-ray during the XPS determination [59] and for the influence of $Mn_2O_3$ modification. As reported by Spassova et al. [25] and Fortunato et al. [60], a redoxy equilibrium between $MnO_x$ and CuO in CuO–$MnO_x$ system is generally observed.

### 3.4. $H_2$-temperature programmed reduction

Interactions between metal oxide and support were interrogated using $H_2$-TPR and TPR profiles of the Cu/Mn–Al catalysts are shown in Fig. 7. A weak $H_2$ consumption peak around 400 °C was observed in the profile of 0.6Mn–Al sample (see Fig. 7). Kapteijn

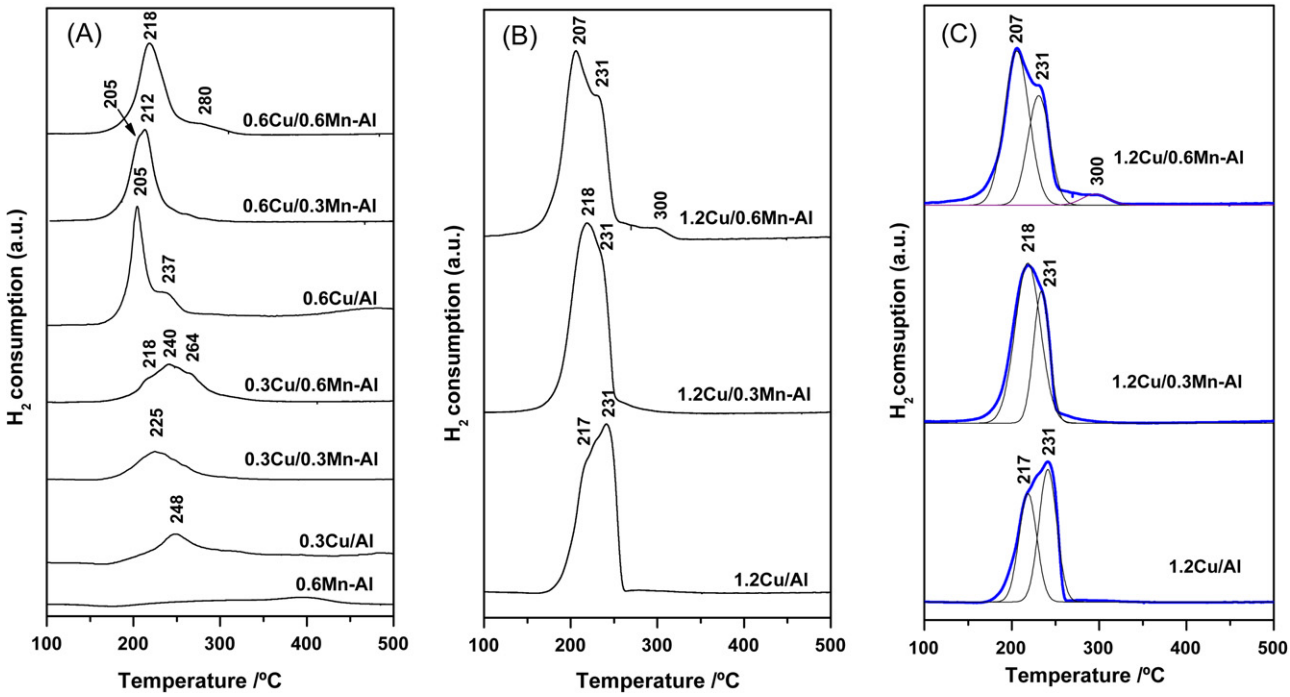


**Fig. 7.** TPR profiles of various Cu/Mn–Al catalysts. (A) 0.3Cu/*y*Mn–Al and 0.6Cu/*y*Mn–Al; (B) 1.2Cu/*y*Mn–Al; (C) PFM results of 1.2Cu/*y*Mn–Al.

et al. [33] studied alumina supported manganese oxide catalysts. They found that a $H_2$ consumption peak around 380 °C in the TPR profile of 6% Mn–Al sample and assigned to the reduction of $Mn_2O_3$ to $Mn_3O_4$. In contrast, Cu/Mn–Al catalysts showed marked different TPR patterns, which were closely related to the loading amounts of copper oxide and manganese oxide. For 0.3Cu/Al, a $H_2$ consumption peak appeared at 248 °C, which assigned to the reduction of dispersed copper oxide species incorporated into the C-layer's octahedral vacant sites of γ-$Al_2O_3$ [61]. In the profile of 0.3Cu/0.3Mn–Al, a $H_2$ consumption peak was observed at 225 °C, which is slightly lower as compared to 0.3Cu/Al. The reduction behaviors of 0.3Cu/0.6Mn–Al became complicated and three $H_2$ consumption peaks were observed at ~216, 240 and 264 °C. Buciuman et al. [62] studied the reducible properties of $CuMn_2O_4$ and the mixture of CuO and $Mn_2O_3$. They found that copper oxide reduced at about 260 and 320 °C in the presence of $Mn_2O_3$ and $CuMn_2O_4$. Therefore, it is reasonable to assign the peak at 264 °C as the reduction of CuO occupied the tetrahedral vacancy sites of the epitaxial layer of $Mn_2O_3$.

The reduction behaviors of supported CuO are closely linked to CuO loading amount. In comparison with 0.3Cu/Al, a much stronger $H_2$ consumption peak at 205 °C with a shoulder at 237 °C was observed in the TPR profile of 0.6Cu/Al. For 0.6Cu/0.3Mn–Al, a $H_2$ consumption peak at 212 °C with a shoulder at 205 °C appeared. As for 0.6Cu/0.6Mn–Al, in contrast, only a $H_2$ consumption peak at 218 °C was observed. For γ-$Al_2O_3$ supported CuO, the reduction peaks at 205 and 237 °C are attributed to the reduction of copper oxide incorporated into the D-layer and C-layer's octahedral vacant sites of γ-$Al_2O_3$ respectively [61]. Upon $Mn_2O_3$ modification, the reduction peak at 237 °C disappeared, indicating that the CuO incorporated into the octahedral vacancy sites of C-layer of γ-$Al_2O_3$ disappeared due to epitaxil layer of $Mn_2O_3$ occupied the vacancy sites. The reduction peaks of 0.3Cu/*y*Mn–Al and 0.6Cu/*y*Mn–Al were slightly lower than those of 0.3Cu/Al and 0.6Cu/Al, indicating that $Mn_2O_3$ modification can promote the reduction of copper oxide.

The TPR profiles of the 1.2Cu/*y*Mn–Al catalysts are compared in Fig. 7(B). For all catalysts, two $H_2$ consumption peaks around 218 and 231 °C were observed, which could be attributed to the reduction of dispersed copper oxide and to the reduction of crystalline CuO. In addition, the intensities of $H_2$ consumption peaks for the catalysts were markedly increased in comparison with 0.3Cu/*y*Mn–Al and 0.6Cu/*y*Mn–Al samples. Moreover, increasing the manganese oxide loading led to the increase of $H_2$ consumption for the reduction of dispersed copper oxide but to decrease for that of crystalline CuO, indicative of increased dispersed CuO content and decreased crystalline CuO content with the increase of $Mn_2O_3$. To clearly elucidate the influence of manganese oxide on the reduction of copper oxide, the $H_2$ reduction peaks in the TPR profiles of 1.2Cu/*y*Mn–Al catalysts were deconvoluted and the fitting curves and resultant peak areas are compared in Fig. 7(C) and Table 2. As listed in Table 2, the total peak areas of 1.2Cu/Al, 1.2Cu/0.3Mn–Al, and 1.2Cu/0.6Mn–Al were found to be 175.9 to 192.5 and 231.5 a.u. respectively, suggesting that manganese oxide was partially reduced at low reduction temperature (<300 °C) due to the hydrogen spillover effect. In addition, the peak areas of dispersed CuO in 1.2Cu/Al, 1.2Cu/0.3Mn–Al, and 1.2Cu/0.6Mn–Al were calculated to be 76.4, 130.2 and 142 a.u. respectively, reflecting increased content of dispersed CuO with $Mn_2O_3$ loading. The opposite trend was observed for crystalline CuO. The results are well consistent with XRD results.

**Table 2**
The peak areas of the TPR profiles of various 1.2Cu/*y*Mn–Al catalysts.

| Samples | Peak area (a.u.) | | |
|---|---|---|---|
| | 1.2Cu/Al | 1.2Cu/0.3Mn–Al | 1.2Cu/0.6Mn–Al |
| Total | 175.9 | 192.5 | 231.5 |
| $Mn_2O_3$ | | 16.6 | 55.6 |
| Peak at ~210 °C | 76.4 | 130.2 | 142 |
| Peak at ~230 °C | 93.4 | 61.5 | 86.2 |
| Peak at ~300 °C | | | 7.6 |
| CuO at ~210 °C | | | 142 |
| CuO at ~230 °C | 76.4 | 130.2 | 30.6 |
| $CuMnO_x$ | 93.4 | 40.4 | 7.6 |

### 3.5. In situ Fourier transform infrared spectroscopy studies

To verify the valent states of copper oxides in the Cu/Mn–Al catalysts, in situ IR spectroscopy of CO adsorption over the catalysts was conducted, and the IR spectra of CO adsorption on 0.6Cu/*y*Mn–Al and 0.3Mn–Al are compared in Fig. 8. Generally, one group of peaks in the range of 1300–1700 $cm^{-1}$ and the other at about 2102 $cm^{-1}$ were observed in the spectra over these catalysts. The bands at 1375 and 1559 $cm^{-1}$ corresponding to the symmetrical vibration ($\nu_s(COO^-)$) and asymmetrical vibration ($\nu_{as}(COO^-)$) of the carboxylates [63,64], and 1456 and 1623 $cm^{-1}$ corresponding to the symmetrical vibration ($\nu_s(COO)$) and asymmetrical vibration ($\nu_{as}(COO)$) of the bicarbonates [63–65]. For all of the catalysts, the bands at 1375, 1459, 1559 and 1623 $cm^{-1}$ were detected, and the intensity of the bands at 1459 and 1559 $cm^{-1}$ did not change while that of the band at 1623 $cm^{-1}$ decreased during the increase of the temperature, indicating the bicarbonates are unstable. The band at about 2100 $cm^{-1}$ corresponding to the CO molecular adsorbed on the sites of $Cu^+$, $Mn^{3+}$, $Al^{3+}$ cations, then the discussion is focused on this region. For 0.3Mn–Al, no absorption peaks were observed at the region between 2000 and 2200 $cm^{-1}$, indicating that CO is unabsorbed as single molecule on $Mn^{3+}$ and/or $Al^{3+}$. For 0.6Cu/Al, a band around 2100 $cm^{-1}$ was observed at 25 °C, which is assigned to CO absorption on the $Cu^+$ [64,66–69]. The intensity of this band increased as the temperature reached the maximum at 250 °C and disappeared at 300 °C, suggesting that some $Cu^{2+}$ species were reduced to $Cu^+$ before 250 °C during the absorption test and the absorbed CO desorbed as the temperature further increased. It can be concluded that the amount of $Cu^+$ species reached the maximum over 0.6Cu/Al at 250 °C. In addition, the band shifted from 2100 to 2114 $cm^{-1}$ from 25 to 250 °C, indicative of a slightly blue shift of CO absorption due to the increasing temperature. A similar IR band position of CO absorption exception a new band at 2174 $cm^{-1}$ was observed over the 0.6Cu/0.3Mn–Al and 0.6Cu/0.6Mn–Al samples at 25 and 50 °C. This can be attributed to $Mn^{2+}$–CO [64] because of some $Mn^{3+}$ reduced in CO stream. This band disappeared at 100 °C, indicating the species is unstable. The intensity of the band at about 2100 $cm^{-1}$ increasing with

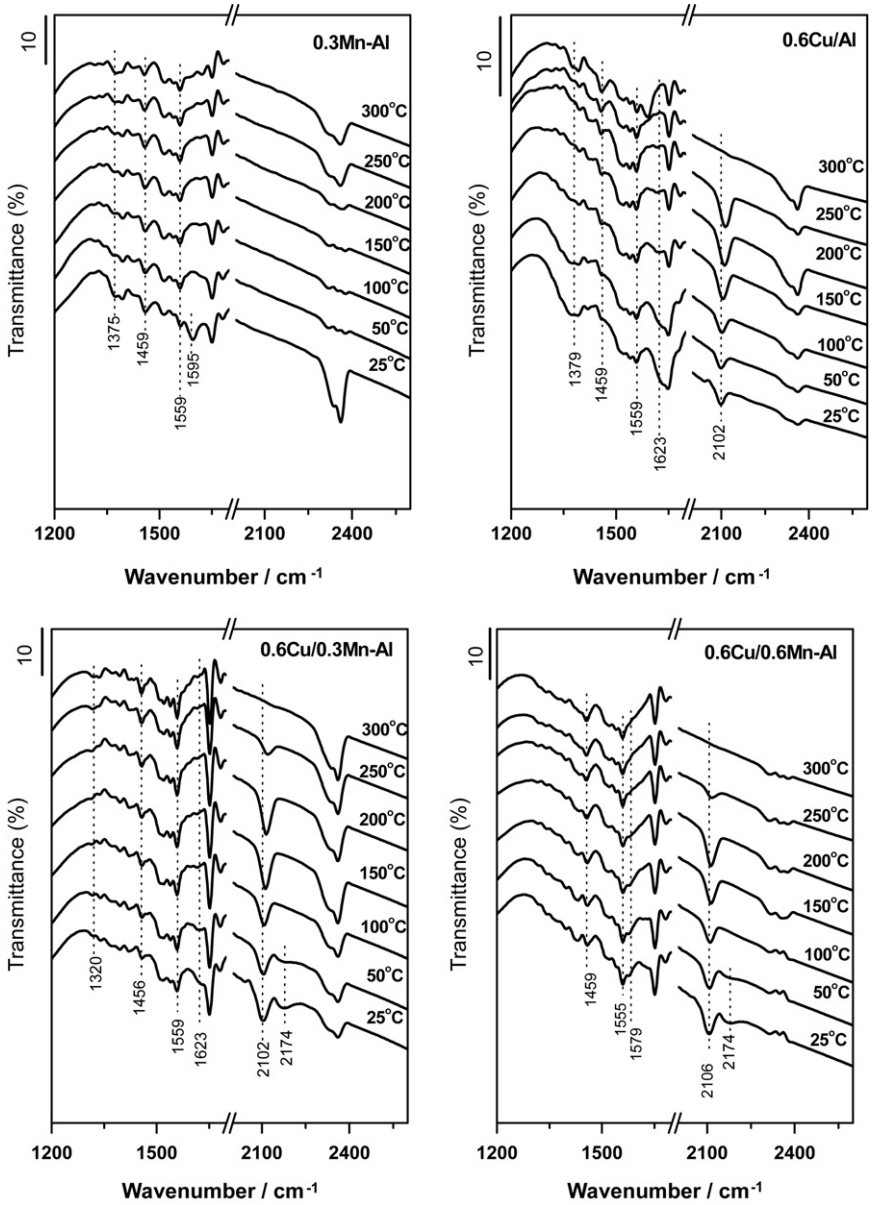


**Fig. 8.** IR spectra of CO adsorbed on 0.6Cu/*y*Mn–Al catalysts.

temperature and reaching the maximum at 200 °C is indicative of the amount of $Cu^+$ species reaching the maximum at 200 °C, implying $Mn_2O_3$ enhanced the reducibility of copper oxide which is consistent with the $H_2$-TPR results. Spassova et al. [25] studied mixed CuO–$MnO_x$ oxides and found a redoxy equilibrium between CuO and $MnO_x$ as $Cu^{2+} + Mn^{3+} \leftrightarrow Cu^+ + Mn^{4+}$. Fortunato et al. [60] reported a similar result from the study of spinel $CuMn_2O_4$ oxide. A similar position and trend were observed from the CO adsorption over 0.3Cu/*y*Mn–Al and 1.2Cu/*y*Mn–Al samples, the detailed results are not shown here.

IR spectra of NO adsorption on 0.6Cu/*y*Mn–Al catalysts are shown in Fig. 9. For 0.6Cu/Al, IR bands around 1907, 1848, 1628, 1600 and 1292 $cm^{-1}$ appeared at 25 °C. The IR bands at 1907 and 1848 $cm^{-1}$ are assigned to the vibration of gas NO molecular [70,71] and the bands at 1628, 1600 and 1292 $cm^{-1}$ to the NO absorption as bridging bidentate nitrate species of which 1629 and 1600 $cm^{-1}$ corresponding to $\nu$(N═O) and 1293 $cm^{-1}$ corresponding to $\nu$(O–N–O) [72,73], the scheme is shown in Fig. 9 also. With the increase of temperature, the bands at 1628 and 1600 $cm^{-1}$ corresponding to bridging bidentate nitrate species disappeared while two new bands at 1576 and 1525 $cm^{-1}$ corresponding to $\nu$(N═O) and $\nu_{as}(NO_2)$ of nitro [73,74] were observed, and the intensity of the band at 1293 $cm^{-1}$ corresponding to $\nu$(O–N–O) of nitro increased substantially, indicating the NO adsorption as bridging bidentate nitrate species at low temperature transform to nitro species at high temperature. For the 0.6Cu/0.3Mn–Al and 0.6Cu/0.6Mn–Al samples, a similar phenomenon was observed. NO adsorption of 0.3Cu/*y*Mn–Al and 1.2Cu/*y*Mn–Al samples shows similar trend as that of 0.6Cu/*y*Mn–Al, the spectra are not shown here.

CO-IR results indicate that $Mn_2O_3$ can promote the reduction of $Cu^{2+}$ to $Cu^+$, and NO-IR results show that the influence of $Mn_2O_3$ is negligible. To further investigate the role of $Mn_2O_3$, in situ IR spectroscopy of NO–CO co-adsorption over the 0.6Cu/*y*Mn–Al catalysts was conducted and the IR spectra are compiled in Fig. 10. For 0.3Mn–Al, several weak IR bands at 1629, 1600 and 1293 $cm^{-1}$ attributing to the NO absorption as bridging bidentate nitrate

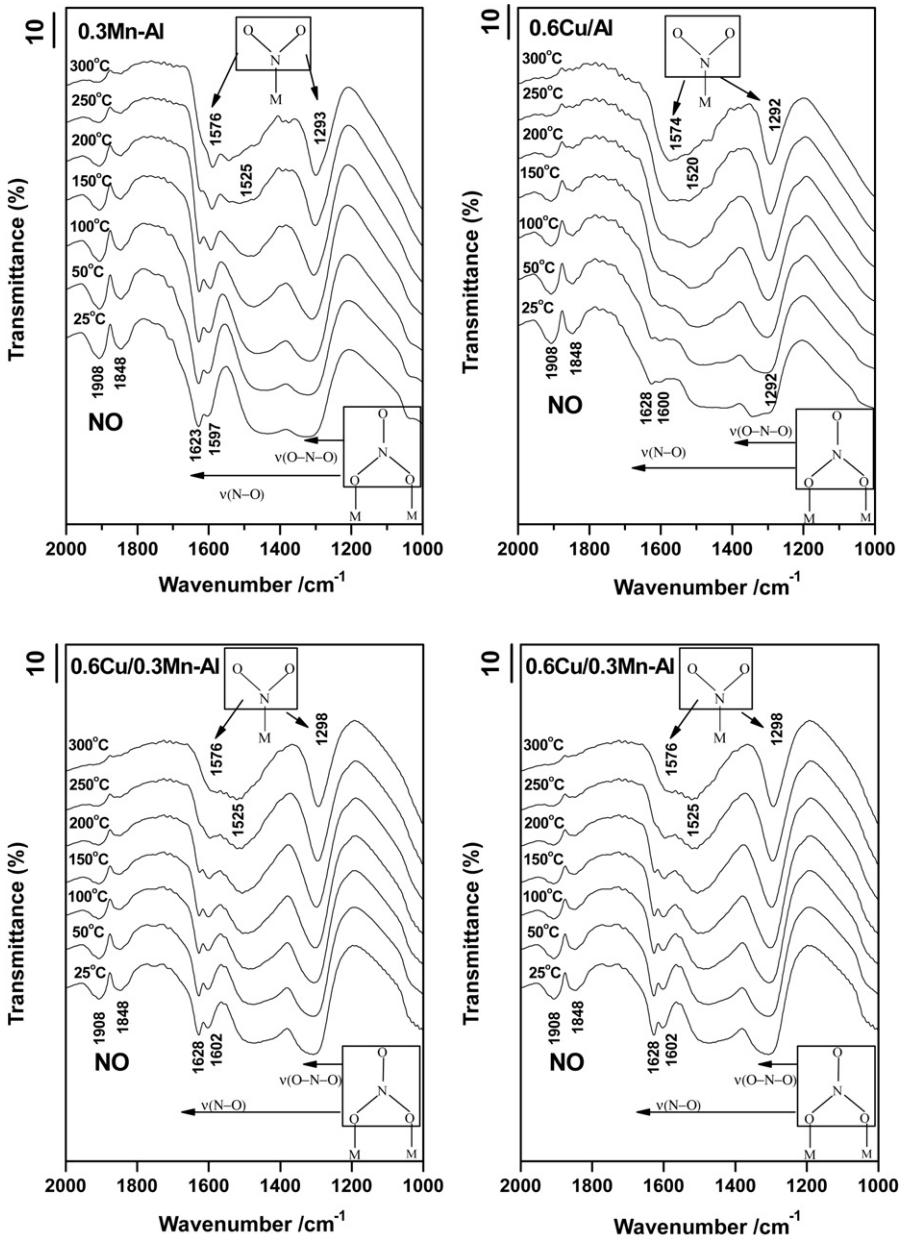


**Fig. 9.** IR spectra of NO adsorbed on 0.6Cu/*y*Mn–Al catalysts.

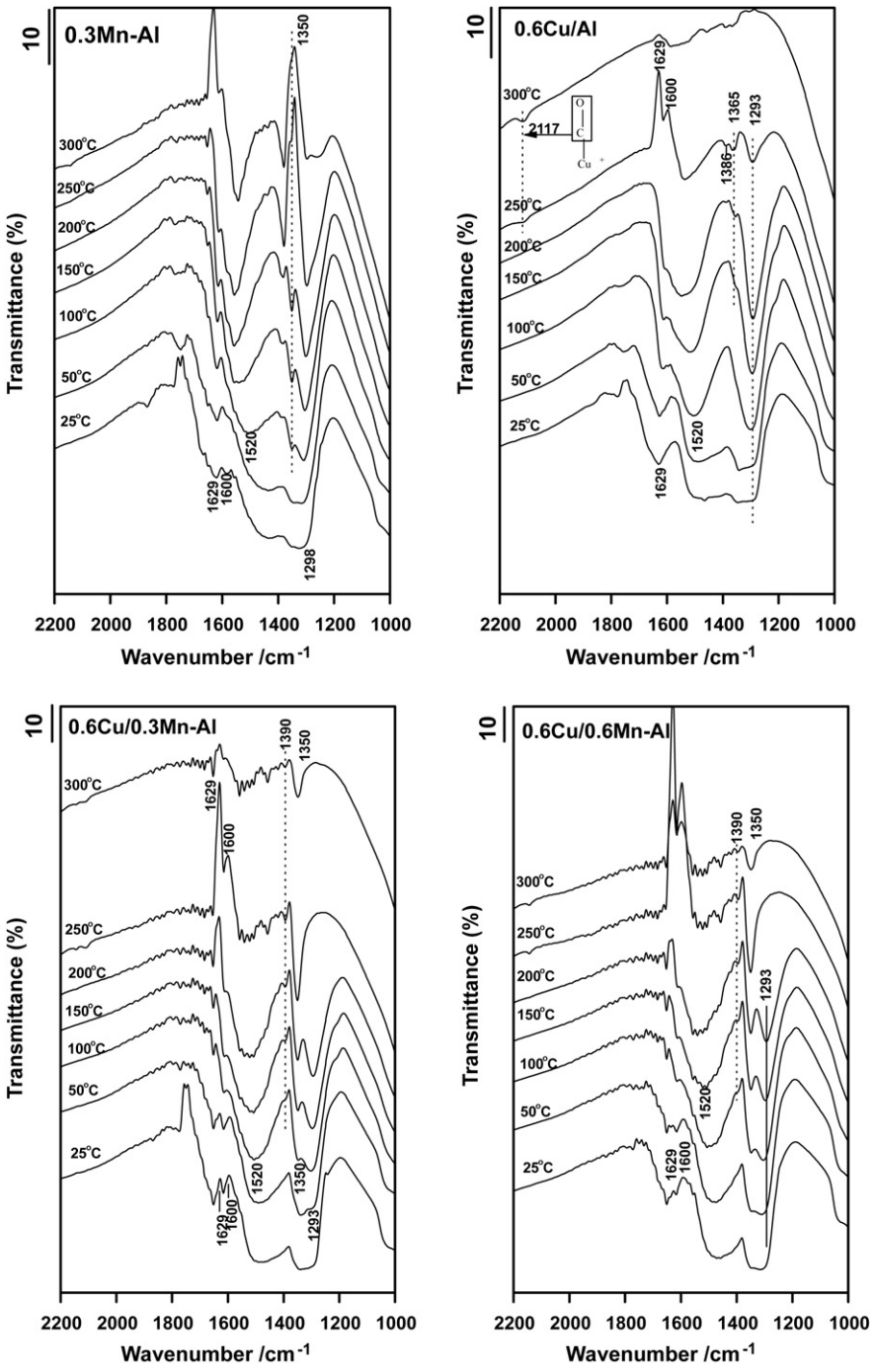


**Fig. 10.** IR spectra of CO and NO co-adsorbed on 0.6Cu/*y*Mn–Al catalysts.

species were observed at 25 °C, and the intensity of bands at 1629 and 1600 $cm^{-1}$ decreased while a new band at 1350 $cm^{-1}$ appeared at 100 °C. The intensity of bands at 1350 and 1293 $cm^{-1}$ increased with temperature increase. For 0.6Cu/Al, a weak band at 1629 $cm^{-1}$ was detected at 25 °C, which decreased with the temperature increase while a band at 1520 $cm^{-1}$ appeared at 100 °C. As the temperature increased to 200 °C, the intensity of bands at 1520 and 1293 $cm^{-1}$ increased but decreased as temperature further increased to 250 °C, at the same time, positive peaks at 1629 and 1600 $cm^{-1}$ appeared, indicating the amount of the nitrate/nitro species on the catalyst surface lower than that of background adopted because part of NO were reduced by CO surface at this temperature. At the same temperature, a weak IR band at 2117 $cm^{-1}$ attributed to CO absorption on $Cu^{+}$ appeared, and a very weak band at 1386 $cm^{-1}$ attributed to nitrate appeared but no band at 1350 $cm^{-1}$ were detected. For the 0.6Cu/0.3Mn–Al and 0.6Cu/0.6Mn–Al samples, a similar phenomenon was observed, but the band at 1350 $cm^{-1}$ appeared at 50 °C and the intensity increased with the temperature, indicating this band correlation with $Mn^{3+}$ species. The attribution of this band is unclear, Venkov et al. [73] detected this band (1351 $cm^{-1}$) as $C_2H_4$ adsorption on $Cu/Al_2O_3$ catalyst but they did not discuss the attribution. Hadjiivanov et al. [75] also detected this band (1354 $cm^{-1}$) in the $H_2O$ and NO co-adsorption on H-ZSM-5, and they assigned it to the vibration of the H-bonded zeolite hydroxyl. This band was mentioned by Hadjiivanov [72] in the review of the NO adsorption on oxide sur-

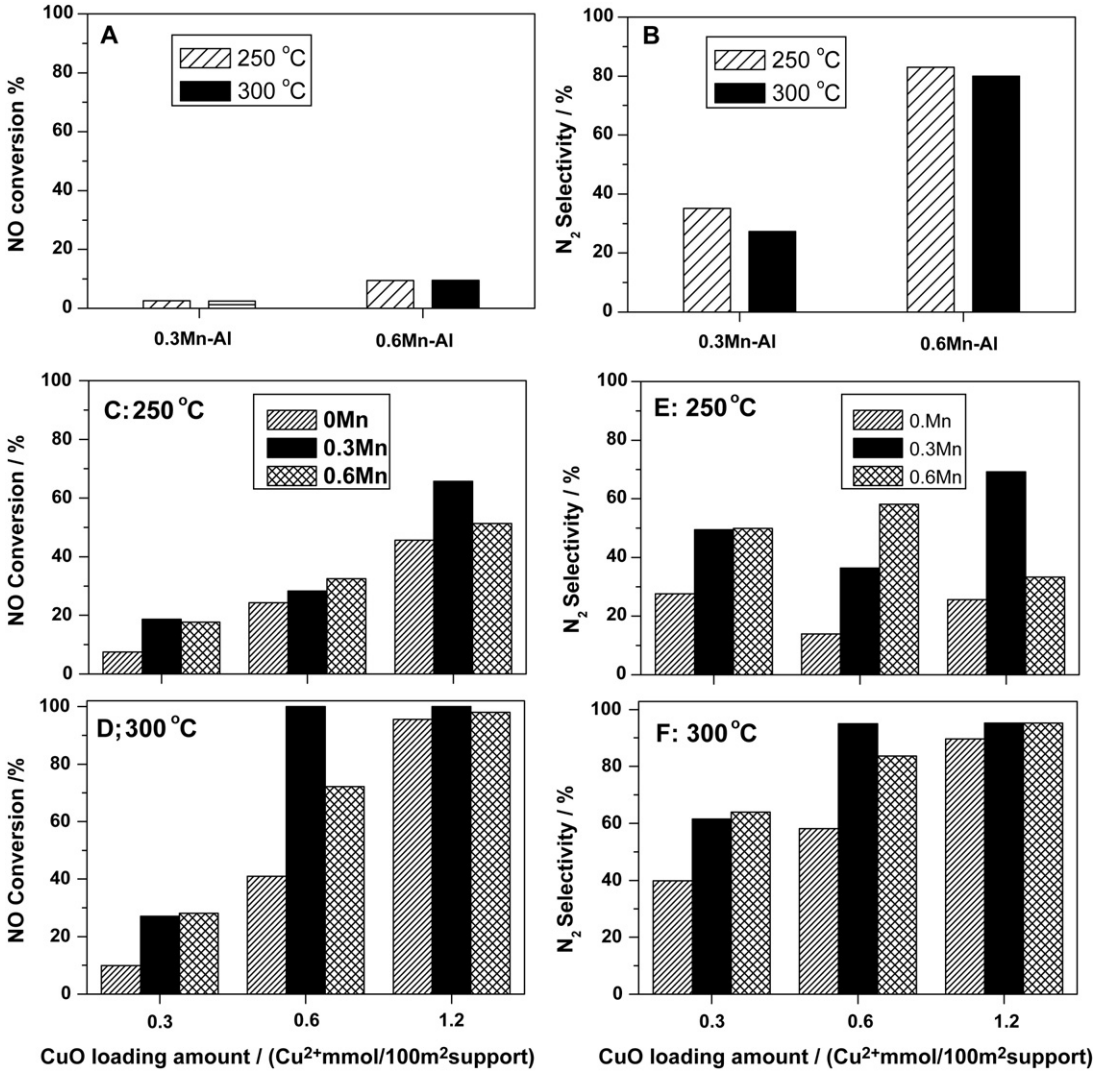


**Fig. 11.** Activities of *y*Mn–Al supports and various Cu/Mn–Al catalysts.

face, as nitro compound adsorbed on the surface of metal cation, $\nu_s(NO_2)$ at 1350–1320 $cm^{-1}$ would be detectable. Accordingly, this band is attributed to the $\nu(NO_2)$ of nitro ($NO_2^-$) adsorption on $Mn^{3+}$ [70,72].

### 3.6. NO reduction by CO

NO conversions and $N_2$ selectivity of Cu/Mn–Al catalysts at 250 and 300 °C are shown in Fig. 11. For comparison, the activities of *y*Mn/Al samples are also shown in Fig. 11(A) and (B). For the 0.3Mn–Al and 0.6Mn–Al samples, the NO conversions were even lower than 10% at both temperatures whatever the loading of manganese oxide, but the $N_2$ selectivity was promoted as the manganese oxide loading increased. As the reaction temperature increased from 250 to 300 °C, the NO conversions over the 0.3Mn–Al sample were 2.6%, 2.5% and those over 0.6Mn–Al sample were 9.5% and 9.6% respectively, indicating that the effect of reaction temperature over *y*Mn–Al could be neglected.

In contrast, for the Cu/Mn–Al catalysts, the conversion of NO is strongly dependent on the reaction temperature and the loading amounts of copper oxide and manganese oxide. The NO conversion was enhanced by increasing the reaction temperature, e.g. the NO conversions over 0.3Cu/Al, 0.3Cu/0.3Mn–Al and 0.3Cu/0.6Mn–Al were 7.5%, 18.6% and 17.7% at 250 °C while were 9.9%, 27.1% and 28.1% at 300 °C, respectively. A similar trend was observed over 0.6Cu/*y*Mn–Al and 1.2Cu/*y*Mn–Al catalysts. It should be noted that the NO conversions achieved about 100% at 300 °C over the 0.6Cu/0.3Mn–Al and 1.2Cu/0.3Mn–Al catalysts. Simultaneously, $N_2$ selectivity over these catalysts was also promoted as the reaction temperature increased. Additionally, the NO conversion increased gradually with the loading of copper oxide over *x*Cu/Al catalysts at both reaction temperatures, e.g., NO conversions were 18.6%, 28.3% and 65.7% over the 0.3Cu/0.3Mn–Al, 0.6Cu/0.3Mn–Al, 1.2Cu/0.3Mn–Al catalysts, respectively, at 250 °C. Upon the modification of manganese oxide, both the NO conversion and $N_2$ selectivity were promoted. For example, the NO conversion and $N_2$ selectivity over 0.6Cu/Al were 40% and 58.2% which increased to 100% and 95% respectively over 0.6Cu/0.3Mn–Al at 300 °C. However, the changes in the NO conversions are complicated which was strongly dependent on the loading amounts of copper oxide and manganese oxide and reaction temperatures. With the loading of copper oxide at 0.6 and 1.2 mmol, the NO conversions did not change evidently upon 0.3Mn–Al and 0.6Mn–Al support at 300 °C, especially for the 0.3Mn–Al support; they both reached 100%, indicating that dispersed copper oxide species were active components. Moreover, NO conversion was associated with the reaction temperature. At 250 °C, maximum NO conversion was observed over 1.2Cu/0.3Mn–Al catalyst, but maximum conversion

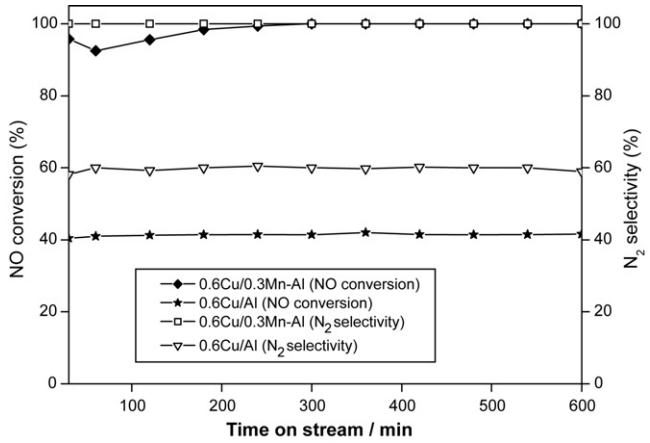


**Fig. 12.** Study of the stability of 0.6Cu/Al and 0.6Cu/0.3Mn–Al catalysts for NO–CO reaction at 300 °C.

was achieved over 0.6Cu/0.3Mn–Al catalyst at 300 °C. $N_2$ selectivity did not evidently depend on the loading amounts of copper oxide and manganese oxide at 250 °C, whereas it was slightly promoted when manganese oxide was presented. At 300 °C, the promoting effect induced by increasing the loading amount of copper oxide and the presence of manganese oxide was more obvious. However, it is worth noting that for the 0.3Mn–Al and 0.6Mn–Al support the $N_2$ selectivity is very nearly. The activity of the 0.6Cu/Al and 0.6Cu/0.3Mn–Al catalysts as a function of time on stream is compiled in Fig. 12. The NO conversion and $N_2$ selectivity of both catalysts keep invariableness during the test time, indicating that these catalysts are stable in this reaction condition and the redoxy recycle between copper oxide and manganese oxide reached a balance.

Combining the structure of the catalysts and the activity results, the dispersion capacity of copper oxide is enhanced over the manganese modified $\gamma$-$Al_2O_3$ support. The presence of $Mn^{3+}$ can promote $Cu^{2+}$ transfer to $Cu^{+}$ in Cu/Mn–Al catalysts, which can improve the CO molecular absorption capability over the catalysts. And $Mn^{3+}$ can adsorb nitro ($NO_2^-$) species, which may be the intermediate of this reaction. So the activities of Cu/Al catalysts are promoted by manganese oxide modification. Therefore, it can be concluded that dispersed copper oxide species in Cu/Al catalysts is the main active species toward NO reduction by CO. The role of dispersed manganese oxide can be attributed to promoting the dispersion of copper oxide species. Additionally, the redoxy system $Cu^{2+} + Mn^{3+} \leftrightarrow Cu^{+} + Mn^{4+}$ also plays an important role in this reaction.

## 4. Conclusion

The catalytic activities of CuO supported on manganese oxide modified $\gamma$-$Al_2O_3$ for NO reduction by CO were investigated. Compared with the CuO/$\gamma$-$Al_2O_3$ catalysts, $Mn_2O_3$ modified catalysts are proved to be active in terms of the NO conversions and $N_2$ selectivity. The catalytic behavior of the Cu/Mn–Al catalyst for NO reduction by CO is associated with the properties of $\gamma$-$Al_2O_3$, loading amount and reducibility of CuO and the reaction temperature. Manganese oxide modified $\gamma$-$Al_2O_3$ can promote the dispersion capacity of CuO on the support because an epitaxil $Mn_2O_3$ monolayer formed on the $\gamma$-$Al_2O_3$ surface resulting in the tetrahedral vacant sites of surface $Mn_2O_3$ can be preferentially occupied by $Cu^{2+}$. Manganese oxide modification promotes the reducibility of CuO and enhances the CO adsorption abilities on Cu/Al catalysts because $Cu^{2+} + Mn^{3+} \leftrightarrow Cu^{+} + Mn^{4+}$ redoxy system results in $Cu^{+}$ formed in Cu/Mn–Al catalysts. Therefore, the NO conversions and $N_2$ selectivity of Cu/Al catalysts in NO–CO reaction are promoted by the modification of manganese oxide.

## Acknowledgments

This work was financially supported by the National Natural Science Foundation of China (Nos. 20873060 and 20973091). The authors also thank Dr. Fei Gao for the helpful discussion.

## References

[1] J. Nováková, Appl. Catal. B: Environ. 30 (2001) 445–457.
[2] J.M.D. Cónsul, I. Costilla, C.E. Gigola, I.M. Baibich, Appl. Catal. A: Gen. 339 (2008) 151–158.
[3] H. Inomata, M. Shimokawabe, M. Arai, Appl. Catal. A: Gen. 332 (2007) 146–152.
[4] N.W. Cant, D.C. Chamber, I.O.Y. Liu, Appl. Catal. B: Environ. 60 (2005) 57–63.
[5] I. Nakamura, Y. Kobayashi, H. Hamada, T. Fujitani, Surf. Sci. 600 (2006) 3235–3242.
[6] L. Ilieva, G. Pantaleo, J.W. Sobczak, I. Ivanov, A.M. Venezia, D. Andreeva, Appl. Catal. B: Environ. 76 (2007) 107–114.
[7] J.T. Kummer, Prog. Eng. Combust. Sci. 6 (1980) 177–199.
[8] W.S. Kijlstra, D.S. Brands, E.K. Poels, A. Bliek, J. Catal. 171 (1997) 208–218.
[9] N.B. Stankova, M.S. Khristova, D.R. Mehandjiev, J. Colloid Interface Sci. 241 (2001) 439–447.
[10] I. Spassova, M. Khristova, R. Nickolov, D. Mehandjiev, J. Colloid Interface Sci. 320 (2008) 186–193.
[11] M. Kang, E.D. Park, J.M. Kim, J.E. Yie, Appl. Catal. A: Gen. 327 (2007) 261–269.
[12] M. Shelef, K. Otto, J. Catal. 10 (1968) 408–412.
[13] F. Kapteijn, L. Singoredjo, A. Andreini, J.A. Moulijn, Appl. Catal. B: Environ. 3 (1994) 173–189.
[14] T. Yamashita, A. Vannice, J. Catal. 163 (1996) 158–168.
[15] T. Yamashita, A. Vannice, J. Catal. 161 (1996) 254–262.
[16] R. Nickolov, N. Stankova, M. Khristova, D. Mehandjiev, J. Colloid Interface Sci. 265 (2003) 121–128.
[17] M.M. Pineda, S. Castillo, M. Asomoza, R. Gomez, J. Therm. Anal. Calorim. 73 (2003) 341–346.
[18] X.Y. Jiang, L.P. Lou, Y.X. Chen, X.M. Zheng, J. Mol. Catal. A: Chem. 197 (2003) 193–205.
[19] M. Khristova, B. Ivanov, I. Spassova, T. Spassov, Catal. Lett. 119 (2007) 79–86.
[20] D. Panayotov, M. Khristova, M. Velikova, Appl. Catal. B: Environ. 9 (1996) 107–132.
[21] D. Stoyanova, M. Christova, P. Dimitrova, J. Marinova, N. Kasabova, D. Panayotov, Appl. Catal. B: Environ. 17 (1998) 233–244.
[22] D. Panayotov, React. Kinet. Catal. Lett. 58 (1996) 73–78.
[23] A.B. Lamb, W.C. Bray, J.C.W. Frazer, J. Ind. Eng. Chem. 12 (1920) 213–221.
[24] C. Yoon, D.L. Cocke, J. Catal. 113 (1988) 267–280.
[25] I. Spassova, M. Khristova, D. Panayotov, D. Mehandjiev, J. Catal. 185 (1999) 43–57.
[26] S. Veprek, D.L. Cocke, S. Kehl, H.R. Oswald, J. Catal. 100 (1986) 250–263.
[27] G.J. Hutchings, A.A. Mirzaei, R.W. Joyner, M.R.H. Siddiqui, S.H. Taylor, Appl. Catal. A: Gen. 166 (1998) 143–152.
[28] B.L. Yang, S.F. Chan, W.S. Chang, Y.Z. Chen, J. Catal. 130 (1991) 52–61.
[29] J. Papavasiliou, G. Avgouropoulos, T. Ioannides, J. Catal. 251 (2007) 7–20.
[30] M.I. Zaki, M.A. Hasan, L. Pasupulety, Appl. Catal. A: Gen. 198 (2000) 247–259.
[31] D.G. Stoilova, R.N. Nickolov, K.T. Cheshkova, J. Colloid Interface Sci. 228 (2000) 24–31.
[32] M.A. Vicente, C. Belver, R. Trujillano, V. Rivesa, A.C. Álvarez, J.-F. Lambert, S.A. Korili, L.M. Gandía, A. Gil, Appl. Catal. A: Gen. 267 (2004) 47–58.
[33] F. Kapteijn, A.D.V. Langeveld, J.A. Moulijn, A. Andreïni, M.A. Vuurman, A.M. Turek, J.M. Jehng, I.E. Wachs, J. Catal. 150 (1994) 94–104.
[34] Y.C. Xie, Y.Q. Tang, Adv. Catal. 37 (1990) 1–43.
[35] L. Dong, Y. Chen, J. Chem. Soc. Faraday Trans. 92 (1996) 4589–4593.
[36] Y. Chen, L.F. Zhang, Catal. Lett. 12 (1992) 51–62.
[37] Y.X. Zhu, J.Y. Yang, H.J. Yan, Nat. Gas Chem. Indus. (Chinese) 18 (1993) 6–9.
[38] W.S. Xia, H.L. Wan, Y. Chen, J. Mol. Catal. A: Chem. 138 (1999) 185–195.
[39] X.W. Li, H.Q. Wan, B. Liu, L.J. Yang, H.Y. Zhu, H.L. Chen, X. Zhao, K.Q. Sun, L. Dong, Y. Chen, Catal. Commun. 10 (2009) 741–745.
[40] Z. Wang, H.Q. Wan, B. Liu, X. Zhao, X.W. Li, H.Y. Zhu, X. Xu, F.Y. Ji, K.Q. Sun, L. Dong, Y. Chen, J. Colloid Interface Sci. 320 (2008) 520–526.
[41] Y.H. Hu, T.D. Liu, M.M. Shen, H.Y. Zhu, S.T. Wei, X. Hong, W.P. Ding, L. Dong, Y. Chen, J. Solid State Chem. 170 (2003) 58–67.
[42] K. Faungnawakij, N. Shimoda, T. Fukunaga, R. Kikuchi, K. Eguchi, Appl. Catal. A: Gen. 341 (2008) 139–145.
[43] L.Y. Chen, T. Horiuchi, T. Osaki, T. Mori, Appl. Catal. B: Environ. 23 (1999) 259–269.
[44] S. Velu, K. Suzuki, M. Okazaki, M.P. Kapoor, T. Osaki, F. Ohashi, J. Catal. 194 (2000) 373–384.
[45] K.M. Parida, S.S. Dash, S. Singha, Appl. Catal. A: Gen. 351 (2008) 59–67.
[46] W.S. Kijlstra, E.K. Poels, A. Bliek, B.M. Weckhuysen, R.A. Schoonheydt, J. Phys. Chem. B 101 (1997) 309–316.
[47] G.A. Schuit, B.C. Gates, AIChE J. 19 (1973) 417–438.
[48] Y. Chen, L.F. Zhang, J.F. Lin, Y.S. Jin, Catal. Sci. Technol. 1 (1991) 291–298.

[49] J.P. Beaufils, Y. Barbaux, J. Chim. Phys. 78 (1981) 347–352.
[50] B.R. Strohmeier, D.M. Hercules, J. Phys. Chem. 88 (1984) 4922–4929.
[51] A. Wöllner, F. Lange, H. Schmelz, H. Knözinger, Appl. Catal. A: Gen. 94 (1993) 181–203.
[52] M. Oku, K. Hirokawa, S. Ikeda, J. Electron. Spectrosc. Relat. Phenom. 7 (1975) 465–473.
[53] V.A.M. Brabers, F.M.V. Setten, P.S.A. Knapen, J. Solid. State Chem. 49 (1983) 93–98.
[54] I.M. Cabrera, M.L. Granados, J.L.G. Fierro, J. Catal. 210 (2002) 285–294.
[55] L. Kundakovic, M.F. Stephanopoulos, Appl. Catal. A: Gen. 171 (1998) 13–29.
[56] F. Severino, J.L. Brito, J. Laine, J.L.G. Fierro, A.L. Agudo, J. Catal. 177 (1998) 82–95, and the reference therein.
[57] W.J. Shan, Z.C. Feng, Z.L. Li, J. Zhang, W.J. Shen, C. Li, J. Catal. 228 (2004) 206–217.
[58] W. Liu, M. Flytzani-Stephanopoulos, J. Catal. 153 (1995) 317–332.
[59] H.Y. Zhu, M.M. Shen, Y. Kong, J.M. Hong, Y.H. Hu, T.D. Liu, L. Dong, Y. Chen, C. Jian, Z. Liu, J. Mol. Catal. A: Chem. 219 (2004) 155–164.
[60] G. Fortunato, H.R. Oswald, A. Reller, J. Mater. Chem. 11 (2001) 905–911.
[61] H.Q. Wan, Z. Wang, J. Zhu, X.W. Li, B. Liu, F. Gao, L. Dong, Y. Chen, Appl. Catal. B: Environ. 79 (2008) 254–261.
[62] F.C. Buciuman, F. Patcas, T. Hahn, Chem. Eng. Process 38 (1999) 563–569.
[63] K.K. Bando, K. Sayama, H. Kusama, K. Okabe, H. Arakawa, Appl. Catal. A: Gen. 165 (1997) 391–409.
[64] K.I. Hadjiivanov, G.N. Vayssilov, Adv. Catal. 47 (2002) 307–511.
[65] L.J. Liu, J.G. Cai, L. Qi, Q. Yu, K.Q. Sun, B. Liu, F. Gao, L. Dong, Y. Chen, J. Mol. Catal. A: Chem. 327 (2010) 1–11.
[66] R. Hierl, H. Knozinger, H.P. Urbach, J. Catal. 69 (1981) 475–486.
[67] M.B. Padley, C.H. Rochester, G.J. Hutchings, F. King, J. Catal. 148 (1994) 438–452.
[68] J.W. Bijsterbosch, F. Kapteijn, J.A. Moulijn, J. Mol. Catal. 74 (1992) 193–205.
[69] O. Dulaurent, X. Courtois, V. Perrichon, D. Bianchi, J. Phys. Chem. B 104 (2000) 6001–6011.
[70] S.J. Huang, A.B. Walters, M.A. Vannice, J. Catal. 192 (2000) 29–47.
[71] Y.W. Chi, S.S.C. Chuang, J. Catal. 190 (2000) 75–91.
[72] K.I. Hadjiivanov, Catal. Rev. Sci. Eng. 42 (2000) 71–144.
[73] T. Venkov, M. Dimitrov, K.I. Hadjiivanov, J. Mole. Catal. A 243 (2006) 8–16.
[74] Q. Yu, L.J. Liu, L.H. Dong, D. Li, B. Liu, F. Gao, K.Q. Sun, L. Dong, Y. Chen, Appl. Catal. B: Environ. 96 (2010) 350–360.
[75] K. Hadjiivanov, J. Saussey, J.L. Freysz, J.C. Lavalley, Catal. Lett. 52 (1998) 103–108.